Eur. Phys. J. D **18**, 19–26 (2002)
DOI: 10.1140/e10053-002-0016-5

THE EUROPEAN PHYSICAL JOURNAL D
EDP Sciences

Floquet study of ionization and high-order harmonic generation for a hydrogen atom in high-frequency laser fields

T. Cheng[1,a], J. Liu[2], and S. Chen[2]

[1] Laboratory of Optical Physics, Institute of Physics and Center for Condensed Matter Physics, Chinese Academy of Science, Beijing 100080, P.R. China
[2] Center for nonlinear studies, Institute of Applied Physics and Computational Mathematics, P.O. Box 8009-28, Beijing 100088, P.R. China

Received 6 June 2001 and Received in final form 31 August 2001

Abstract. In this paper, we investigate the dynamics of a hydrogen atom in high-frequency (several atomic units) super strong (up to several tens of atomic units) laser fields within the high frequency Floquet theory framework. The ionization rate, ionization spectrum, angular distribution and high-order harmonic generation are all investigated. Our studies reveal the universal behavior of the total ionization rate, excess-photon ionization spectrum and angular distribution of the ionization rate in the stabilization regime, and achieve a deep insight into the dynamics of high-order harmonic generation in the stabilization regime.

PACS. 32.80.Rm Multiphoton ionization and excitation to highly excited states (e.g., Rydberg states) – 32.80.Fb Photoionization of atoms and ions – 42.50.Hz Strong-field excitation of optical transitions in quantum systems; multi-photon processes; dynamic Stark shift

1 Introduction

Great progress has been achieved on the topic of atoms interacting with intense laser fields in recent years [1,2]. Many non-perturbative theories have been developed and proved to be successful in explaining novel experimental observations. Among these theories, the high frequency Floquet theory (HFFT) developed by Gavrila and co-workers [3,4] is one of the most satisfactory theories in the studies of atomic behavior in high frequency laser fields. It has successfully predicted the stabilization phenomenon, and has been extended to various kinds of studies to provide insight into a variety of physical systems [5–11].

On the other hand, various kind of *ab initio* calculation such as the Sturmian-Floquet approach [12], R-matrix theory [13] and time-dependent calculations [14,15] have shown undisputable stabilization in real hydrogen atoms. However, for any real three-dimensional (3D) atom, most studies based on HFFT are either confined to the atomic structures [4,10], or the ionization dynamics under the Born approximation [11]. In reference [5], the ionization dynamics are investigated with the exact first-order HFFT calculations, using a one-dimensional model atom and the model atom has a short range potential. To our knowledge, the systematic first order HFFT study of ionization and especially high-order harmonic generation (HOHG) processes for real three-dimensional laser-atom interacting systems is still lacking. However, in our previous work [16], an iterative scheme for calculating both ionization rate and high-order harmonic generation within the HFFT framework was developed. For a one-dimensional (1D) model atom, we find that we can obtain quite good accuracy with much less numerical burden, compared with the *ab initio* method. In this paper, we extend the above iterative method to the 3D hydrogen atom case and present an intense investigation on the laser-hydrogen system in the high-frequency regime.

This paper is organized as follows: in Section 2, we present our numerical techniques for treating the laser-atom interacting system in the three-dimensional case; in Section 3, we give our numerical results on the total ionization rate, partial ionization rates (excess-photon ionization (EPI) distribution and angular distribution) and the HOHG spectrum; in Section 4 we provide further discussions on the numerical results. The final section contains our concluding remarks.

2 The iterative treatment for a hydrogen atom in high-frequency laser fields

The time-dependent Schrödinger equation (TDSE) of a hydrogen atom interacting with linear polarized (in z-direction) monochromatic laser fields in the

[a] e-mail: taiwangcheng@hotmail.com

Kramers-Henneberger (KH) frame [17] can be written as (throughout this paper, atomic units $m = e = \hbar = 1$ a.u. are used)

$$\mathrm{i}\frac{\partial}{\partial t}\Psi(\mathbf{r},t) = \Big(-\frac{1}{2}\Delta + V\big(\mathbf{r}-\alpha(t)\hat{\mathbf{z}}\big)\Big)\Psi(\mathbf{r},t), \qquad (1)$$

where $V(\mathbf{r}) = -1/|\mathbf{r}|$ is the atomic potential, and $\alpha(t) = E/\omega^2\sin(\omega t) = \alpha_0\sin(\omega t)$ represents the free motion of an electron in the external laser fields, E and ω are the amplitude and frequency of the external field respectively, and $\alpha_0 = E/\omega^2$ represents the free excursion of electrons in the laser fields. Since $\alpha(t)$ is a periodical function, we can expand $V\big(\mathbf{r}-\alpha(t)\hat{\mathbf{z}}\big)$ in Fourier series

$$V\big(\mathbf{r}-\alpha(t)\hat{\mathbf{z}}\big) = \sum_n V_n(\mathbf{r})\mathrm{e}^{-\mathrm{i}n\omega t}. \qquad (2)$$

In [16] we have developed an iterative method to seek Floquet type solution

$$\Psi(\mathbf{r},t) = \mathrm{e}^{-\mathrm{i}Et}\psi(\mathbf{r},t) \qquad (3)$$

for equation (1), in which $\psi(\mathbf{r},t) = \psi(\mathbf{r},t+T)$, and $T = 2\pi/\omega$ is the period of the laser fields. The results can be readily written as follows.

(1) Zeroth order: for asymptotically high frequency, we can drop all the time-dependent terms, then $\Psi(\mathbf{r},t) = \mathrm{e}^{-\mathrm{i}E^0t}\psi_0(\mathbf{r})$, in which $\psi_0(\mathbf{r})$ and E^0 are determined by

$$H_0\psi_0(\mathbf{r}) = E^0\psi_0(\mathbf{r}), \qquad (4)$$

$H_0 = -\Delta/2 + V_0(\mathbf{r})$ is the KH Hamiltonian, and the corresponding state ψ_0 is the KH state.

(2) First order:

$$\Psi(\mathbf{r},t) = \mathrm{e}^{-\mathrm{i}E^0t}\left(\psi_0(\mathbf{r}) + {\sum_n}'\delta\psi_n^{(1)}(\mathbf{r})\mathrm{e}^{-\mathrm{i}n\omega t}\right), \qquad (5)$$

here $\sum'$ represents sum over all ns except $n = 0$. $\delta\psi_n^{(1)}(\mathbf{r})(n \neq 0)$ is determined by

$$[(E^0 + n\omega) - H_0]\delta\psi_n^{(1)}(\mathbf{r}) = V_n\psi_0(\mathbf{r}). \qquad (6)$$

We require $\delta\psi_n^{(1)}(\mathbf{r}) \overset{r\to\infty}{\longrightarrow} (1/r)f_n(\hat{\mathbf{r}})\exp[\mathrm{i}(k_nr - \gamma_n\ln 2k_nr)]$ for open channels $n > 0$ (note that we have made the high frequency assumption, *i.e.*, the frequency is higher than the binding energy $-E^0$, so one-photon ionization is always possible), and $\delta\psi_n^{(1)}(\mathbf{r}) \overset{r\to\infty}{\longrightarrow} 0$ for closed channel $n < 0$. k_n is determined from $k_n^2/2 = E^0 + n\omega$, and $\gamma_n = -1/k_n$.

(3) Second order:

$$\Psi(\mathbf{r},t) = \mathrm{e}^{-\mathrm{i}(E^0+\delta^2E)t}\Bigg(\psi_0(\mathbf{r}) + \delta^2\psi_0(\mathbf{r}) + \left({\sum_n}'\delta\psi_n^{(2)}(\mathbf{r})\mathrm{e}^{-\mathrm{i}n\omega t}\right)\Bigg), \qquad (7)$$

here δ^2E is determined by

$$\delta^2E = \left\langle\psi_0\middle|{\sum_n}'V_{-n}\delta\psi_n^{(1)}\right\rangle. \qquad (8)$$

$\delta\psi_n^{(2)}(\mathbf{r})(n \neq 0)$ and $\delta^2\psi_0(\mathbf{r})$ are determined by

$$[(E^0 + n\omega + \delta^2E) - H_0]\delta\psi_n^{(2)}(\mathbf{r}) = V_n\psi_0(\mathbf{r}), \qquad (9)$$

and

$$[E^0 - H_0]\delta^2\psi_0(\mathbf{r}) = -\delta^2E\psi^0 + {\sum_n}'V_{-n}\delta\psi_n^{(1)}. \qquad (10)$$

The boundary conditions for $\delta\psi_n^{(2)}(\mathbf{r})$ are roughly the same as for $\delta\psi_n^{(1)}(\mathbf{r})$, except that for $\delta\psi_n^{(2)}(\mathbf{r})$ the k_n is determined from $k_n^2/2 = E^0 + \delta^2E + n\omega$, and thus $k_n = k_n' - \mathrm{i}k_n''$ (k_n', k_n'' are real and we require $k_n' > k_n'' > 0$), and $\gamma_n = -1/k_n'$.

Due to the fact that the system has cylindrical symmetry, we can expand the wave functions and potential functions in equations (1–10) with the spherical harmonic functions: $F(\mathbf{r}) = \sum_l F_l(r)Y_l(\theta)$, here $Y_l(\theta)$ is the spherical harmonic function and $F_l(r)$ is function of the radial coordinate r only. By using such expansion, we can separate the radial part and angular part of the wave functions and thus greatly simplify the calculation. Now we describe our calculation procedure in some detail.

First, we solve equation (4) to find the KH state ψ_0 and its eigenenergy E^0 (in this paper we only consider the ground state). To do this, we expand $\psi_0(\mathbf{r})$ and $V_0(\mathbf{r})$ with spherical harmonic functions:

$$\psi_0(\mathbf{r}) = \sum_l \psi_{0l}(r)Y_l(\theta), \qquad (11)$$

and

$$V_0(\mathbf{r}) = \sum_l V_{0l}(r)Y_l(\theta), \qquad (12)$$

and then equation (4) can be written as the following coupled differential equations,

$$-\frac{1}{2}\left(\frac{1}{r^2}\frac{\partial}{\partial r}\left(r^2\frac{\partial}{\partial r}\right) - \frac{l(l+1)}{r^2}\right)\psi_{0l} + \sum_{l_1,l_2} C_{l_1,l_2,l}V_{0l_1}\psi_{0l_2} = E^0\psi_{0l}, \quad (l = 0,1,...). \qquad (13)$$

In the above equations

$$C_{l_1,l_2,l} = \sqrt{\frac{(2l_1+1)(2l_2+1)}{4\pi(2L+1)}}|\langle l_10l_20|l0\rangle|^2,$$

and $\langle l_10l_20|l\rangle$ is the Clebsch-Gordan (CG) coefficient. We let $g_{0l}(r) = r\psi_{0l}(r)$, and we will find $g_{0l}(r)$ satisfies:

$$-\frac{1}{2}\left(\frac{\partial^2}{\partial r^2} - \frac{l(l+1)}{r^2}\right)g_{0l} + \sum_{l_1,l_2} C_{l_1,l_2,l}V_{0l_1}g_{0l_2} = E^0g_{0l}, \quad (l = 0,1,...). \qquad (14)$$

In the above equations, we can separate the Hamiltonian into two terms: H_k and H_V, where

$$H_k = -\frac{1}{2}\left(\frac{\partial^2}{\partial r^2} - \frac{l(l+1)}{r^2}\right)$$

acts only on the radial part of the wave function; and $H_V = \sum_{l_1,l_2} C_{l_1,l_2,l} V_{0l_1} g_{0l_2}$ acts only on the angular part of the wave function. Numerically, the above coupled differential equations equals to a two-dimensional eigenvalue problem, so the imaginary time evolution method can be used to obtain the ground state wave function $g_{0l}(r)$ and eigenenergy E^0. Due to the possibility of separating the Hamiltonian into two parts which acting on the radial or angular part respectively, we can use the Peaceman-Rachford alternative method to perform the time evolution.

After the KH ground state is obtained, we turn our attention to equation (6). Again, we expand $\delta\psi_n^{(1)}(r,\theta)$ in spherical harmonic series $\delta\psi_n^{(1)}(r,\theta) = \sum_l \delta\psi_{nl}^{(1)}(r) Y_l(\theta)$ and set $g_{nl}(r) = r\delta\psi_{nl}^{(1)}(r)$, then by the same argument, equation (6) equals to the following coupled differential equations:

$$(E^0 + n\omega - H_k) g_{nl} - H_V g_{nl} = \sum_{l_1,l_2} C_{l_1,l_2,l} V_{nl_1} g_{0l_2}, \quad (l = 0, 1, ...) \quad (15)$$

here V_{nl} is the lth spherical harmonic component of $V_n(r,\theta)$, *i.e.*, $V_n(r,\theta) = \sum_l V_{nl}(r) Y_l(\theta)$. To obtain g_{nl}, we use an iterative procedure, the $(i+1)$th results can be solved from the ith results from the following equation,

$$(E^0 + n\omega - H_k) g_{nl}^{i+1} - C_{0,l,l} V_{00} g_{nl}^{i+1} = \sum_{l_1,l_2} C_{l_1,l_2,l} V_{nl_1} g_{0l_2}^{i} + \sum_{l_1',l_2} C_{l_1,l_2,l} V_{0l_1} g_{nl_2}^{i}, \quad (l = 0, 1, ...). \quad (16)$$

In the above equations $\sum_{l_1',l_2}$ means summing over different l_1 and l_2 except for the $l_1 = 0$ term. The initial g_{nl}^0 can be set to zero everywhere. We have V_{00} term in the left part of the equations in order to stabilize the convergence of the iterative procedure. The boundary conditions now become $g_{nl}(r) \overset{r\to\infty}{\longrightarrow} f_n \exp[\mathrm{i}(k_n r - \gamma_n l n 2 k_n r)]$ for $n > 0$ and $g_{nl}(r) \overset{r\to\infty}{\longrightarrow} 0$ for $n < 0$. Equations (9, 10) can be solved in the same way as equation (6). Then putting $\delta^2 E$, $\delta\psi_n^{(2)}$ and $\delta^2\psi_0$ in equation (7) will give the Floquet wave function needed.

For the problems specified in this paper, we could also take advantage of the form of the atomic potential to simplify the calculation by noting the following equation:

$$\frac{1}{|\mathbf{r} - \mathbf{r}'|} = \begin{cases} \frac{1}{r'} \sum_l (\frac{r}{r'})^l P_l(\cos\theta) & r < r' \\ \frac{1}{r} \sum_l (\frac{r'}{r})^l P_l(\cos\theta) & r > r'. \end{cases}$$

Here θ is the relative angle between $\mathbf{r}$ and $\mathbf{r}'$. So from equation (12), V_{nl} for different l can be calculated separately.

Having obtained the Floquet wave functions, the physical information of the system can be calculated right away. The ionization rate is just -2 Im $\delta^2 E$. The HOHG can be found by Fourier transforming the dipolar momentum

$$d(t) = \langle \Psi(\mathbf{r},t) | r\cos(\theta) | \Psi(\mathbf{r},t) \rangle, \quad (17)$$

within one period, and the nth harmonic strength can be written as

$$d_n = \sum_m d_{m,m+n} = \sum_m \langle \phi_m(r,\theta) | r\cos(\theta) | \phi_{m+n}(r,\theta) \rangle \cdot \quad (18)$$

Here $\phi_m = \delta\psi_m^{(2)}$ for $m \neq 0$, and $\phi_m = \psi_0 + \delta^2\psi_0$ for $m = 0$. Since we have $\cos(\theta) Y_l = a_l Y_{l+1} + a_{l-1} Y_{l-1}$, with

$$a_l = \frac{l+1}{\sqrt{(2l+1)(2l+3)}},$$

d_n can be obtained directly in the (r,l) space. For the partial ionization distribution, we need to return to the original (r,θ) space. Following equation (40) of reference [4], we have

$$\frac{\mathrm{d}\Gamma_n}{\mathrm{d}\Omega} = k_n' |f_n(R,\theta)|^2 \mathrm{e}^{2k_n'' R} / \sum_n \int_{V(r<R)} |\psi_n^{(2)}|^2 \mathrm{d}V, \quad (19)$$

where R is the boundary set in the r direction and $f_n(R,\theta) = \sum_l f_{nl}(R) Y_l(\theta)$; $\int_{V(r<R)}$ means the integration over the space $r < R$. From equation (19) the angular distribution can be obtained by summing over different n and the EPI spectrum can be obtained from integrating over all directions for different channels n.

3 Numerical results

We now employ the above iterative approach to investigate the ionization and HOHG of the hydrogen atom in a high-frequency monochromatic laser field. Within the HHFT frame, this model has been investigated intensely in the literatures [4,10,11], but except for the atomic structures [10] (dichotomy) and selected results of ionization [5], other information such as the ionization rate, ionization distribution and EPI spectrum are mostly obtained under the Born approximation of the final state [11]. There is no work on the high-order harmonic generation in the stabilization regime within the HFFT to the best of our knowledge. This is due to the fact that the HOHG spectrum cannot be obtained directly from the original HFFT, which is a formal scattering theory. In the following, we will investigate the high frequency laser-hydrogen system with the efficient iterative method presented above. In practical numerical calculations, the grid spacing Δr in the r direction should be small enough in order to incorporate the ionized energetic outgoing electron wave packet; the grid extension in the r direction should be large enough to contain the Floquet wave function; and

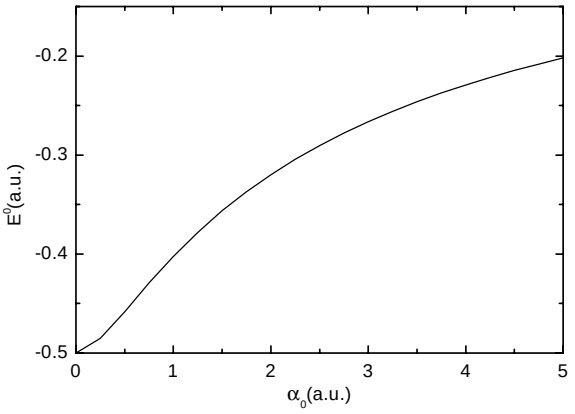

Fig. 1. The KH ground state energy E^0 *versus* α_0.

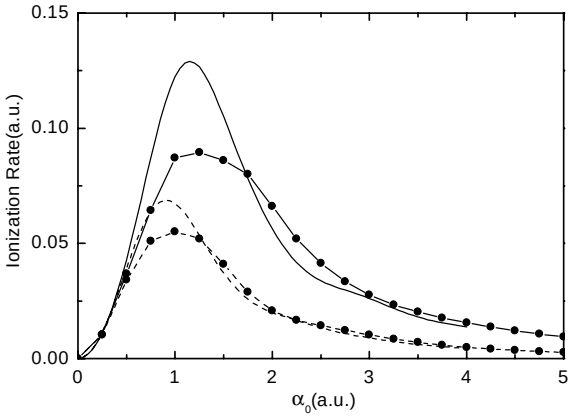

Fig. 2. The ionization rate *versus* α_0 for $\omega = 1$ (solid line with symbol) and $\omega = 2$ (dashed line with symbol); also plotted are results from reference [4], $\omega = 1$ (solid line) and $\omega = 2$ (dashed line).

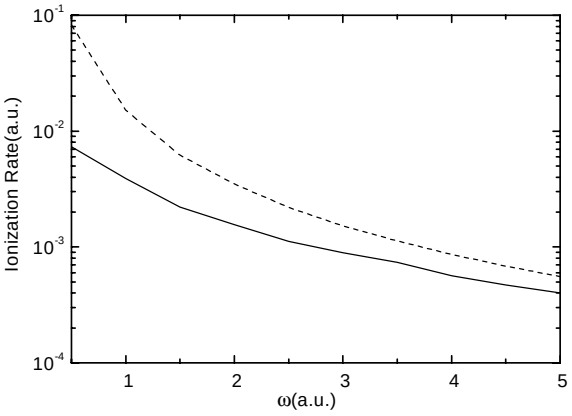

Fig. 3. The ionization rate *versus* ω for $\alpha_0 = 5$, solid line is from the iterative method, and dashed line is from the original the HFFT under the Born approximation.

we should sum over a large range of channels n in order to obtain converged results for the ionization spectrum and the HOHG. Due to the above requirements, we have restricted the number of spherical harmonic basis in our calculations to 32, since we are limited by the computer memory size (we use PCs with 256MB memory). With these parameters, we are able to obtain reliable numerical results for α_0 ranging from 0 to 5. We find that when α_0 increase further, the size of the spherical harmonic function basis which is needed in order to obtain reliable numerical results increases rapidly. The numerous l basis soon make it difficult to do calculations on our computer. Other calculations (either Floquet or wave-propagation) also experience the similar difficulties for large α_0 [4,12]. However, with α_0 as large as 5, we are well in the stabilization regime, and the numerical results can reveal the dynamical characters of ionization and HOHG in the stabilization regime. Hence we confine α_0 in the region $\alpha_0 < 5$ in our calculation. With the parameters used in this paper, the velocity of the electron is still well below light velocity, and the range of the electron's quiver motion is still much smaller than the wavelength. Therefore, relativity effect will not be significant and the dipole approximation is still applicable.

First, we show the eigenenergy of the KH ground state E^0 *versus* α_0 in Figure 1. This agree well with the results obtained in reference [4], *i.e.*, the ionization energy decreases rapidly as α_0 increases. We then present the ionization rate *versus* α_0 in Figure 2 for $\omega = 1$ and $\omega = 2$. Also plotted is the ionization rate obtained from an exact Floquet method [12] (note that these results extend from $\alpha_0 = 0$ to $\alpha_0 = 4$). We find quite a good agreement between our results and the exact results. Our results differ from the exact results only quantitatively and the quantitative difference also diminished for α_0 or ω large (*i.e.*, when the high-frequency condition is fulfilled). From Figure 2 we find that the ionization rate decreases one order of magnitude from $\alpha_0 = 1$ to $\alpha_0 = 5$ for $\omega = 1$ and nearly two orders of magnitude for $\omega = 2$, which clearly demonstrate the atomic stabilization. It should be emphasized that the oscillation behavior of ionization rate *versus* α_0 in the 1D calculation [5,18,19] does not show up in this three-dimensional case. We also demonstrate the frequency dependence of the ionization rate for $\alpha_0 = 5$ in Figure 3, which shows a smooth decrease of ionization rate *versus* frequency.

Secondly, we investigate the partial ionization rate. In the following discussions, we have chosen two typical values for α_0, 1 and 5. As we can observe from Figure 2, at $\alpha_0 = 1$ the ionization rate curve roughly reaches its maximum, while for $\alpha_0 = 5$, we are in the ionization suppression (stabilization) regime. In Figure 4, we show the angular distribution of ionization rate for $\alpha_0 = 1$ and $\alpha_0 = 5$ with $\omega = 2$. Obviously, for $\alpha_0 = 1$ the ionized electrons are congregated around $\pi/4$ off the polarization direction, this is characteristic of angular distribution in ATI regime; while for $\alpha_0 = 5$, the angular distribution become congregated along the direction perpendicular to the polarization direction, and there are more oscillations in the angular distributions. These results are qualitatively in agreement with the analytical results in reference [4]. The frequency dependence of the angular distribution is shown in Figure 5, three frequency are chosen: $\omega = 1$,

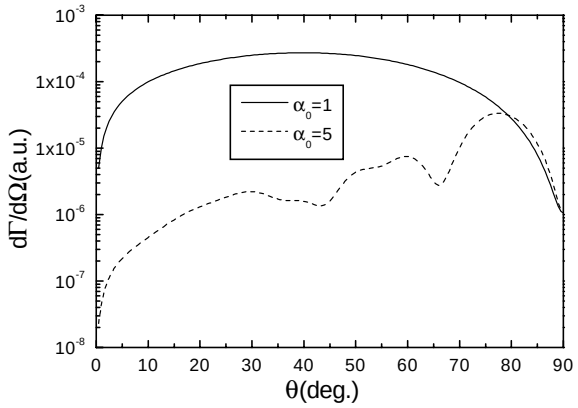

Fig. 4. The angular distribution of the ionization rate for $\alpha_0 = 1$ (solid line) and $\alpha_0 = 5$ (dashed line), $\omega = 2$.

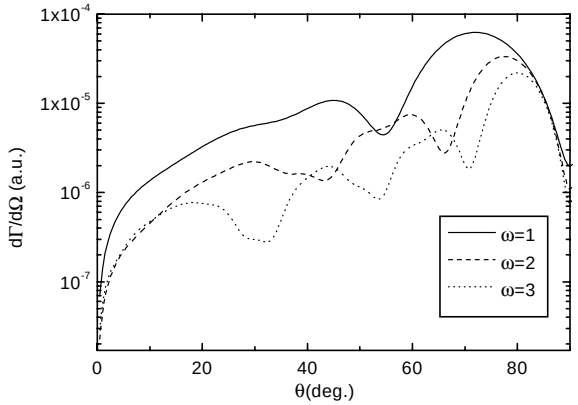

Fig. 5. The angular distribution of the ionization rate for $\omega = 1$ (solid line), $\omega = 2$ (dashed line) and $\omega = 3$ (dotted line), $\alpha_0 = 5$.

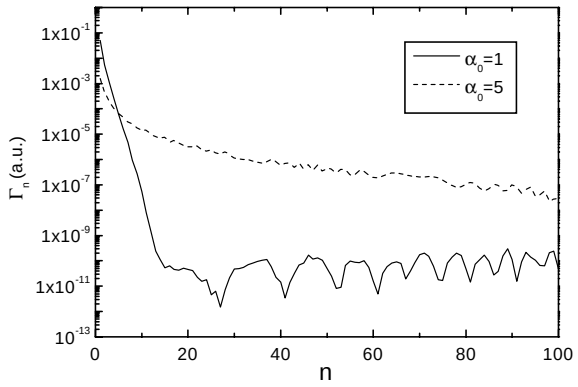

Fig. 6. The EPI spectrum for $\alpha_0 = 1$ (solid line) and $\alpha_0 = 5$ (dashed line), $\omega = 2$.

$\omega = 2$ and $\omega = 3$, and $\alpha_0 = 5$. We find that besides being more and more aligned in the direction perpendicular to the polarization direction, there are more and more oscillations in the angular distributions as ω increases.

We also show the EPI distribution for $\alpha_0 = 1$ and $\alpha_0 = 5$ in Figure 6, the frequency is $\omega = 2$. It is clear that

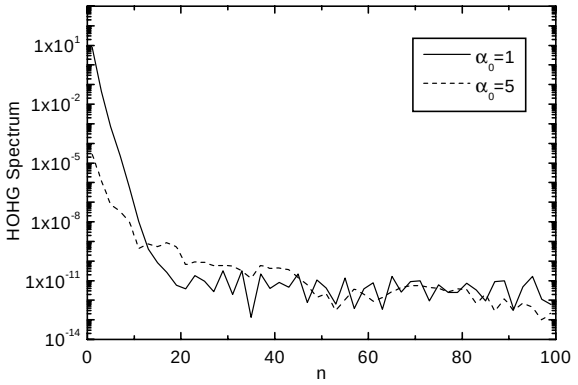

Fig. 7. The HOHG for $\alpha_0 = 1$ (solid line) and $\alpha_0 = 5$ (dashed line), $\omega = 2$.

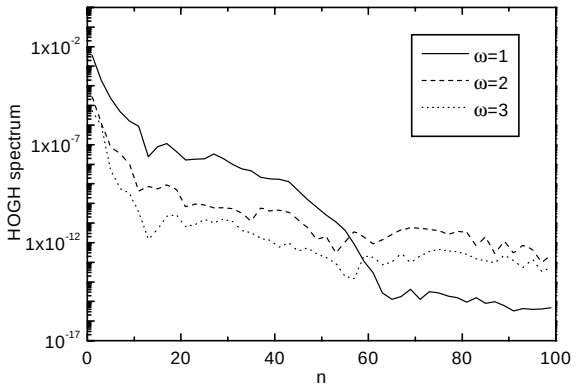

Fig. 8. The HOHG for $\omega = 1$ (solid line), $\omega = 2$ (dashed line) and $\omega = 3$ (dotted line), $\alpha_0 = 5$.

for $\alpha_0 = 1$ the ionization takes place mainly *via* single photon processes and the multi-photon processes can be neglected. For $\alpha_0 = 5$, however, the EPI distribution has a long extended tail, which indicates that in the stabilization regime the contributions from multi-photon process may be also significant.

At last we turn to the HOHG in the stabilization regime. In Figure 7, we show the HOHG spectrum for $\alpha_0 = 1$ and $\alpha_0 = 5$ with $\omega = 2$. We find that roughly, the harmonic intensity will first decrease rapidly and then decrease slowly as the harmonic order n is higher that 10. For $\alpha_0 = 5$ there are also regimes where the harmonic intensity increases with increasing harmonic order n, *i.e.*, there are some oscillations in the HOHG spectrum. Such behavior is also found in the one-dimensional case [16]. In Figure 8, we show the HOHG for $\omega = 1$, $\omega = 2$ and $\omega = 3$ with $\alpha_0 = 5$. We find the same behavior of a rapid decrease followed by a slower decrease for various ω. We find that for $\omega = 1$ there is some kind of "cut off" behavior in the HOHG spectrum, however, before the "cut off", the character of HOHG spectrum holds, and the "cut off" is not an abrupt decrease at some order n. We are not sure if such a "cut off" will occur for $\omega = 2$ and $\omega = 3$, but for these two cases, we find no significant decrease of the harmonic strength up to harmonic orders 100.

The above results confirm that harmonics with very high order can be generated in the stabilization regime (though the efficiency seems not to be very high).

From Figures 7 and 8 we can find the universal characters of the HOHG spectrum in the stabilization regime: (i) the HOHG spectrum shows a rapid decrease for low order harmonics followed by a slowly decreasing regime for the higher order harmonics, no clear "cut off" is found; (ii) in stabilization regime, HOHG are enhanced as decrease for either α_0 or ω.

4 Further discussions and remarks on the numerical results

The decrease of ionization rate has been predicted by the original HFFT from both analytical argument and numerical calculations under the Born approximation. We have plotted the ionization rate calculated under the Born approximation in Figure 3. As is shown in [11], under the Born approximation for linear polarization f_n can be written as:

$$f_n = \frac{1}{\pi k_n^2}\int_{-\pi}^{\pi} \mathrm{e}^{\mathrm{i}n\phi}\mathrm{e}^{\mathrm{i}\alpha(\phi)\hat{\mathbf{z}}\cdot\mathbf{k}_n}\psi_0\big(-\alpha(\phi)\hat{\mathbf{z}}\big)\mathrm{d}\phi. \qquad (20)$$

By putting equation (20) in equation (19), integrating over space and summing over n will give the total ionization rate. However, from Figure 3 we find that, comparing with the ionization rates under the Born approximation, the ionization rate without the Born approximation is smaller. Such discrepancies caused by the Born approximation also exist in the simple one-dimensional model atom [5]. However, from our 3D results presented here, we could not find the multiple stabilization and destabilization behavior suggested by the one-dimensional calculations [18]. This implies that the space average of ionization in different directions suppresses the oscillation behavior. As we will show latter, the mechanism which cause the oscillation of ionization rate *versus* α_0 in the one-dimensional calculation only manifests itself *via* the oscillation in the angular distribution of the ionization rate in 3D case.

We then turn to the partial ionization distribution. The character of angular distribution in stabilization regime, as shown in Figures 4 and 5, is that as the ionization rate decreases, the ionization becomes more and more confined to the direction perpendicular to the polarization directions of the laser fields. This is due to the fact that ionization in the stabilization regime is mainly determined by the momentum transfer process. Since the V_ns are well extended along the polarization direction of the laser fields and thus decrease the forces which can act on the electrons, ionization is more likely to occur when the electron is emitted near the direction perpendicular to the polarization direction, where it will be more likely for the electron to have "hard collision" with the atomic core [20] and hence obtain enough energy to be ionized. As we have said above, though the oscillation identified from the one-dimensional calculations are not found in the three-dimensional calculations, the mechanism which cause the oscillations in one-dimension does show up in the 3D angular distributions. From equations (19, 20), the ionization rate in different directions may be approximately viewed as the ionization rate with different effective α_0, which in turn give rise to the oscillatory behavior in the angular distributions. The mathematical origin of such oscillations can be traced back to the appearance of a Bessel function in the approximation for the ionization rate [11]. The increase in oscillation strength with increasing frequency ω or α_0 is in agreement with the above physical and mathematical pictures.

As for the EPI distribution, from Figure 6, we find that the characteristic of the EPI distribution in the stabilization regime is the long extended tail. From equation (6), Γ_n can be formally expressed as

$$\begin{aligned}\Gamma_n &= -2\mathrm{Im}\big\langle\psi_0\big|V_{-n}\delta\psi_n^{(1)}(\mathbf{r})\big\rangle \\ &= -2\mathrm{Im}\left\langle\psi_0\left|V_{-n}\frac{V_n(\mathbf{r})\psi_0(\mathbf{r})}{E^0 - H_0 + n\omega + \mathrm{i}\epsilon}\right\rangle\right. . \end{aligned} \qquad (21)$$

The ionization rate given by equation (21) is exactly equal to the ionization rate given in [4] which takes a formal scattering form,

$$\Gamma_n = 2\pi{\sum_n}' \mathbf{S}_E\big|\langle u_E|V_n|\psi_0\rangle\big|^2\delta(E_n - E), \qquad (22)$$

where $\mathbf{S}_E$ denotes the integration over energy space, and u_E is the continuum eigenstate of H_0 with eigenenergy E. As shown in reference [21], in the stabilization regime (*i.e.* α_0 is large), V_n's magnitude decrease quite slowly with n. On the other hand, V_n have n nodes within the range of $\pm 2\alpha_0$ on the z-axis. This means that V_n will be more and more oscillatory in coordinate space as n increases. Since $\langle u_E|V_n|\psi_0\rangle$ can be approximately viewed as a Fourier transformation of $V_n|u\rangle$ in energy space, the increase of oscillation in V_n will slow down the decrement of $\langle u_E|V_n|\psi_0\rangle$ with n. So the partial ionization rate Γ_n will decrease slowly for large α_0.

Finally, we turn to the HOHG spectrum. From equation (18), d_n is composed of different terms of $d_{m,m+n}$, since $\phi_0(r,\theta) \approx \psi_0(r,\theta)$ is much larger than $\phi_n(r,\theta) = \delta\psi_n^{(2)}(r,\theta)$ $(n \neq 0)$. At first glance, we may think that the terms which contain ϕ_0 will play a dominant role. If this is true, the nth harmonic strength can be approximately written as,

$$d_n^a = \big\langle\delta\psi_{-n}^{(2)}(\mathbf{r})\big|z\big|\psi_0(\mathbf{r})\big\rangle + \big\langle\psi_0(\mathbf{r})\big|z\big|\delta\psi_n^{(2)}(\mathbf{r})\big\rangle\cdot \qquad (23)$$

We present $|d_n^a|^2$ from equation (23) together with $|d_n|^2$ from equation (18) for $\alpha_0 = 5$ and $\omega = 2$ in Figure 9. $|d_n^a|^2$ only agrees with $|d_n|^2$ at $n = 1$, while for $n > 1$, $|d_n^a|^2$ deviate from $|d_n|^2$ greatly. In fact, if we consider $|d_n^a|^2$ only, we would conclude that there are no HOHG. Further investigations on different terms of $d_{m,m+n}$ show that for high order harmonics, the terms with $m \sim -n/2$, $m \simeq 1$ and $m + n \simeq 1$ are dominant in d_n. To explain the above results, we expand $\delta\psi_n$ with a complete set of KH

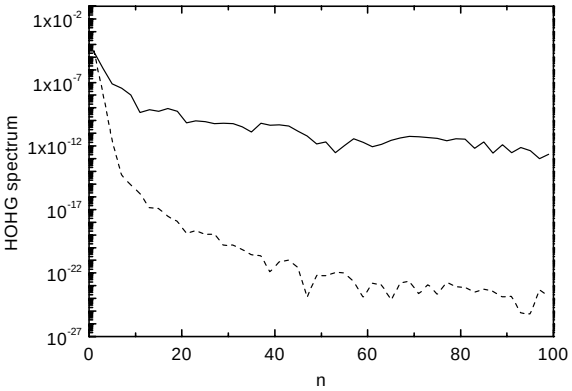

Fig. 9. The HOHG spectrum form equation (18) (solid line) and from equation (23) (dashed line) for $\alpha_0 = 5$ and $\omega = 2$.

states, then

$$d_n^a = \mathbf{S}_E \langle \psi_0 | z | u_E \rangle \langle u_E | V_n \psi_0 \rangle \times \left(\frac{1}{E^2 - E + n\omega} + \frac{1}{E^2 - E - n\omega} \right), \quad (24)$$

where $E^2 = E^0 + \delta^2 E$. In equation (24), we have used the fact that $V_{-n}^* = V_n$ and ψ_0 and z are real. Firstly, $\langle u_E | V_n \psi_0 \rangle$ decrease rapidly with increasing E, so in equation (24), terms with low E will dominant. We can drop E in the denominator of equation (24) if $n\omega$ is large. Then two terms of d_n^a in equation (24) almost cancel each other and d_n^a scales as $(n\omega)^2$, which is very small for large $n\omega$. We find numerically that $d_{0,n}$ and $d_{-n,0}$ almost have the same magnitude but with different sign. Then we turn to the terms of $d_{m,m+n}$ with either m or $m+n$ equal to zero. We combine $d_{m,m+n}$ and $d_{-m-n,-m}$, and obtain

$$d_n = \sum_{-\infty}^{-[\frac{n}{2}]} d_{m,m+n} + d_{-m-n,-m},$$

$d_{m,m+n} + d_{-m-n,-m}$ can be written as,

$$d_{m,m+n} + d_{-m-n,-m} = \mathbf{S}_E \mathbf{S}_{E'} \langle \psi_0 V_m | u_{E'} \rangle \langle u_{E'} | z | u_E \rangle \langle u_E | V_{n+m} \psi_0 \rangle \times \left(\frac{1}{(E_m^2 - E')(E_{m+n}^2 - E)} + \frac{1}{(E_{-m-n}^2 - E)(E_{-m}^2 - E')} \right) \quad (25)$$

where, $E_i^2 = E^2 + \mathrm{i}\omega$. As discussed above, if both $|m|$ and $|m+n|$ are large, then for the integration $\mathbf{S}_E$ and $\mathbf{S}_{E'}$ in equation (25), the contribution from small E and E' will be dominant, and we can approximately drop E and E'. The two terms have the same sign, and will not cancel each other, so equation (25) scales as $m(n+m)\omega^2$ which may be much smaller than $(n\omega)^2$. The reason for the significance of the $m \sim -n/2$ term is that for this case, the numerator is in a symmetric form (note that $V_{-n}^* = V(n)$). This symmetry generally corresponds to a maximum, and thus the numerator is larger than for other choice of ms. As for the terms with $m = 1$ or $m + n = 1$, if E or E' is far away from E_1^2, we can approximately drop E and E' in the denominator of equation (25), and the denominator scales as $n\omega^2$ (which is smaller than $(n\omega)^2$). While for E or E' which is at the vicinity of E_1^2 (note that E_1^2 may not be very large), the integration will approximately generate a delta like function. This makes the denominator scales with $n\omega$ which is much smaller than $(n\omega)^2$. The above two reasons are mixed with each other in real calculations, and contribute to the significance of the $m = 1$ or $m + n = 1$ terms.

The above discussions show that the HOHG picture in the high-frequency stabilization regime differs from the standard ionization-recombination picture [22]. In the HOHG process the direct ionization-recombination process does not play a dominant role, rather, the HOHG process should be viewed as the transition between different Floquet components which are induced by V_n in the oscillating KH frame, as indicated by equation (18) and the above discussions. The dependence of HOHG on α_0 and ω can be explained from equation (25). As we had discussed above, the contribution form the low energy part is dominant in equation (25), and for low E and E', decreasing ω and α_0 will make the denominator decrease and numerator increase, and thus increase the harmonic generation. The slow decreasing of the magnitude of the high-order harmonics can be understood as follows: in equation (25), from the discussions above, we find that the denominator may scale with n as slowly as $1/n$, and the numerator will decrease slowly with n, thus as a whole, the magnitude of high-order harmonics decrease slowly with increasing harmonic order n.

5 Conclusion

In summary, using an efficient numerical technique developed recently, we make a thorough discussion on the ionization and HOHG dynamics in the stabilization regime within the Floquet formalism. Our study reveals the universal properties of ionization rate, angular distribution and EPI distribution in the stabilization regime. Moreover, we have calculated the HOHG in the stabilization regime and provide a novel physical picture of the HOHG for an atom in a high-frequency laser fields. We hope these theoretical studies will stimulate the experimental works on atomic stabilization.

This project is supported by the strong field 973 Project. One of us, T. Cheng, thanks Prof. R.M. Potvliege for kindly giving us his numerical data.

References

1. M. Protopapas, C.H. Keitel, P.L. Knight, Rep. Prog. Phys. **60**, 389 (1997).
2. C.J. Joachain, M. Dörr, N.J. Kylstra, Adv. At. Mol. Opt. Phys. **42**, 225 (2000).

3. M. Gavrila, J.I. Kaminsky, Phys. Rev. Lett. **52**, 614 (1984).
4. M. Gavrila, in *Atoms in intense laser fields*, edited by M. Gavrila (Academic, New York, 1992).
5. M. Marinescu, M. Gavrila, Phys. Rev. A **53**, 2513 (1996).
6. E. van Duijn, M. Gavrila, H.G. Muller, Phys. Rev. Lett. **77**, 3759 (1996).
7. M. Gavrila, J. Shertzer, Phys. Rev. A **53**, 3431 (1996).
8. J.C. Wells, I. Simbotin, M. Gavrila, Phys. Rev. A **56**, 3961 (1997).
9. A.M. Ermolaev, J. Phys. B **31**, L65 (1998).
10. M. Pont, N.R. Walet, M. Gavrila, C.W. MaCurdy, Phys. Rev. Lett. **61**, 939 (1988).
11. M. Pont, Phys. Rev. A **44**, 2152 (1991).
12. R.M. Potvliege, R. Shakeshaft, in *Atoms in intense laser fields*, edited by M. Gavrila (Academic, New York, 1992).
13. M. Dörr, P.G. Purke, C.J. Joachain, C.J. Noble, J. Purvis, M. Terao-Dunseath, J. Phys. B **26**, L275 (1993).
14. K.C. Kulander, K.J. Schafer, J.L. Krause, Phys. Rev. Lett. **66**, 2601 (1991).
15. O. Latinne, C.J. Joachain, M. Dörr, Europhys. Lett. **26**, 333 (1994).
16. T. Cheng, J. Liu, S.G. Chen, Phys. Rev. A **62**, 033402 (2000).
17. W.C. Henneberger, Phys. Rev. Lett. **21**, 838 (1968).
18. T. Millack, J. Phys. B **26**, 4777 (1993).
19. T. Cheng, J. Liu, S. Chen, Phys. Rev. A **59**, 1451 (1999).
20. M. Pont, M. Gavrila, Phys. Rev. A **44**, R4110 (1991).
21. B. Sundaram, R.V. Jensen, Phys. Rev. A **47**, 1415 (1993).
22. P.B. Corkum, Phys. Rev. Lett. **71**, 1994 (1993).